

Extension of Babinet's relations to reflective metasurfaces: Application to the simultaneous control of wavefront and polarization

Takayoshi Fujikawa and Toshihiro Nakanishi

Department of Electronic Science and Engineering, Kyoto University, Kyoto 615-8510, Japan.

(Dated: August 20, 2024)

We extend Babinet's relations, which are originally derived for transmissive metasurfaces, to reflective metasurfaces embedding planar metallic structures in a substrate containing a reflection mirror. To verify the extended Babinet's relations, we investigate two types of reflective metasurfaces embedding self-complementary structures, which produce π -phase difference between two orthogonal linear polarizations under specific conditions required for the extended Babinet's relations. Both theoretical and experimental studies demonstrate a metasurface-based half-wave plate with a reflective metasurface including single self-complementary structures in the terahertz regions. In addition, we study a reflective metasurface with embedded self-complementary structures with phase gradient in reflection, and demonstrate simultaneous implementation of anomalous reflection and polarization conversion with high efficiency.

I. INTRODUCTION

Metamaterials and metasurfaces are artificial media composed of subwavelength structures known as meta-atoms and can be utilized to control electromagnetic wave propagation and polarization [1–3]. The characteristics of metamaterials depend crucially on the structural symmetry of the meta-atoms [4]. For example, metamaterials with broken mirror-symmetry structures exhibit chiral responses [5–9], while those with anisotropic structures exhibit birefringence. Various types of anisotropic metamaterials have been proposed to realize the functions of quarter and half-wave plates, which induce a phase difference between the two orthogonal linear polarizations [10–17]. The wavefront of the incident waves can be controlled in addition to the polarization by introducing a phase gradient into the metasurface [18, 19]. Simultaneous control of the wavefront and polarization has been previously reported using spatial distribution of various anisotropic meta-atoms with different orientations [20–25].

Single-layer transmissive metasurfaces composed of planar metallic structures have been extensively investigated to control transmission waves in various frequency regions, and Babinet's principle has been widely employed in the design of planar structures [26, 27]. The transmission coefficients of the original metallic structures for linear polarization and its complementary structures for orthogonal polarization are linked by simple equations, referred to as Babinet's relations. Babinet's relations were applied to the design of reconfigurable polarization devices using metasurfaces incorporated with phase changing materials, which are introduced to switch between metallic structures and their complementary structures [28–31]. In addition, unique properties of self-complementary structures can be applied to frequency-independent responses [32] and quarter-wave plates [33]. Single-layer transmissive metasurfaces, however, suffer substantial reflection loss, as discussed in Sec. II. On the other hand, reflective metasurfaces composed of planar

metallic structures and a reflective mirror provide a solution to significantly improve the efficiency. In this paper, we compare a transmissive metasurface composed of planar metallic structures with a reflective metasurface composed of the same metallic structures embedded in a substrate and a reflection mirror, and derive conditions in which relations similar to conventional Babinet's relations are satisfied for reflective metasurfaces in the latter part of Sec. II.

According to the extended Babinet's relations, the difference between the reflection phases for two orthogonal linear polarizations is always π for reflective metasurfaces with self-complementary structures under the derived conditions. In other words, the reflective metasurface functions as a half-wave plate. To test this hypothesis, we design a reflective metasurface composed of self-complementary structures and a reflective mirror, which operates in the terahertz regime, and demonstrate a metasurface-based half-wave plate both experimentally and using electromagnetic simulations in Sec. III. Furthermore, we apply the extended Babinet's relations to phase-gradient metasurfaces with spatially varying reflection phases. We design a reflective metasurface that includes eight types of self-complementary structures, thus realizing a linear phase gradient in a specific direction, and demonstrate an anomalous reflection with polarization conversion caused by phase retardation between the two orthogonal polarizations in Sec. IV. This simultaneous control of wavefront and polarization is a unique property derived from the extended Babinet's relations. The extended Babinet's relations may pave the way for efficient multifunctional metasurfaces such as reconfigurable intelligent surfaces [34–37] and polarization-encoded metasurfaces [38, 39].

II. EXTENSION OF BABINET'S RELATIONS TO REFLECTIVE METASURFACE

First, the conventional Babinet's relations for transmissive metasurfaces are reviewed. Suppose a metasur-

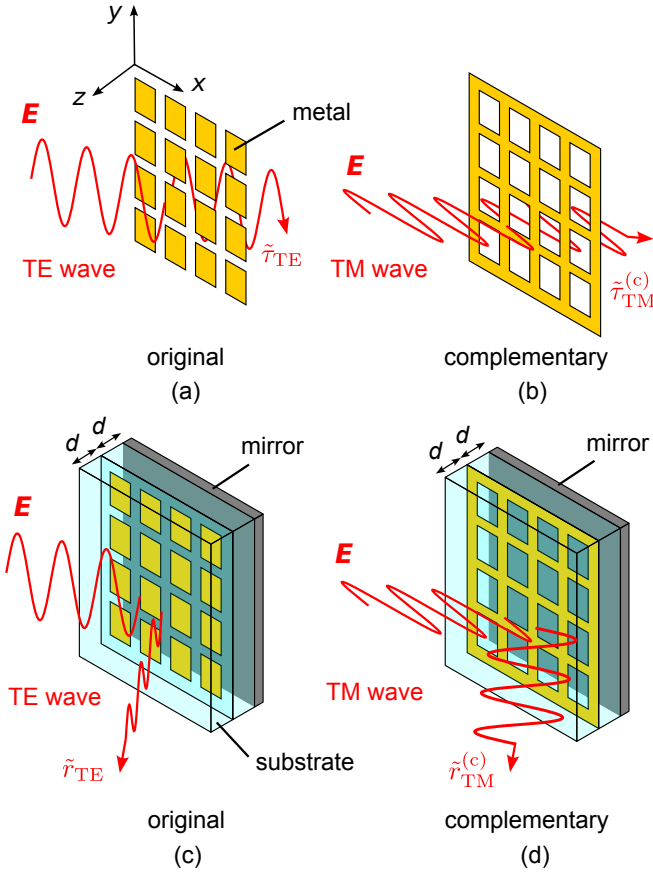


FIG. 1. Electromagnetic response of (a) planar metallic structures and (b) complementary structures. Electromagnetic response of a reflective metasurface embedding (c) planar metallic structures and (d) complementary structures.

face with thin metallic structures located on the $z = 0$ plane is illuminated by TE waves with y -polarization, as shown in Fig. 1(a). Additionally, we assume that the anisotropic axes are aligned in x - and y -directions and the periodicity of the structures is sufficiently small such that diffraction does not occur. Under these conditions, the incident TE waves are separated into two paths as transmitted TE waves and reflected TE waves without diffraction. Next, we consider the interaction between TM waves and a complementary metasurface obtained using the impedance inversion given by $Z_s^{(c)} = Z^2/[4Z_s(x, y)]$, where Z is the wave impedance of the surrounding medium and $Z_s(x, y)$ denotes the local impedance of the original metasurface shown in Fig. 1(a). If the original metasurface comprises a perfect electric conductor $Z_s(x, y) = 0$ and the insulation holes $Z_s(x, y) \rightarrow \infty$, the complementary metasurface can be obtained by swapping the metallic and insulating parts, as shown in Fig. 1(b). It is known that Babinet's principle links the transmission coefficient $\tilde{\tau}_{TE}$ for the original metasurface with the transmission coefficient $\tilde{\tau}_{TM}^{(c)}$ for the

complementary metasurface as follows [27]:

$$\tilde{\tau}_{TE} + \tilde{\tau}_{TM}^{(c)} = 1. \quad (1)$$

A similar relationship is derived by exchanging the TE and TM waves as

$$\tilde{\tau}_{TM} + \tilde{\tau}_{TE}^{(c)} = 1. \quad (2)$$

These relations are referred to as Babinet's relations for transmissive metasurfaces.

In this paper, we propose the reflective metasurface shown in Fig. 1(c). The metasurface embeds metallic planar structures identical to Fig. 1(a) in a substrate with the refractive index n whose backside is covered with a metallic mirror. The reflection coefficient \tilde{r}_i ($i = TE, TM$) in Fig. 1(c) is connected to the transmission coefficient $\tilde{\tau}_i$ and reflection coefficient $\tilde{\rho}_i$ of the metallic planar structure as shown in Fig. 1(a). The same relationship holds for complementary structures, as shown in Fig. 1(b) and a reflective metasurface embedding the structure, as shown in Fig. 1(d). In this section, first, the normal incidence of waves is considered for simplicity. From analyses using transfer matrices, which are presented in Appendix A, we obtain the reflection coefficient \tilde{r}_i under a condition $kd = \pi/2$, where k is the wavenumber in the substrate, as follows:

$$\tilde{r}_i = -\frac{(n+2)\tilde{\tau}_i - 2}{(n-2)\tilde{\tau}_i + 2}, \quad (3)$$

which shows that the reflection coefficient for Fig. 1(c) is expressed as a Möbius transformation of the transmission coefficient $\tilde{\tau}_i$ for the embedded metallic structures. Under the condition $n = 2$, the above relationship is reduced to

$$\tilde{r}_i = -2\left(\tilde{\tau}_i - \frac{1}{2}\right). \quad (4)$$

The same relationship is expected for a reflective metasurface shown in Fig. 1(d), embedding a complementary structure, as shown in Fig. 1(b), and the reflection coefficient is given by $\tilde{r}_i^{(c)} = -2(\tilde{\tau}_i^{(c)} - 1/2)$. Hence, Eqs. (1) and (2) yield the following relations:

$$\tilde{r}_{TE} + \tilde{r}_{TM}^{(c)} = 0, \quad (5)$$

$$\tilde{r}_{TM} + \tilde{r}_{TE}^{(c)} = 0. \quad (6)$$

These relationships can be regarded as Babinet's relations extended to reflective metasurfaces. Note that the relations hold under specific conditions for the refractive index $n = 2$ and thickness $2d = \pi/k$ for the substrate. For oblique incidence, the condition $2d$ is modified to $2d = \pi/(k \cos \theta)$, where θ is the refraction angle in the substrate, as shown in Appendix B.

We reconsider Babinet's relations for transmissive and reflective metasurfaces by representing the transmission and reflection coefficients on a complex plane. For an arbitrary transmissive metasurface composed of planar

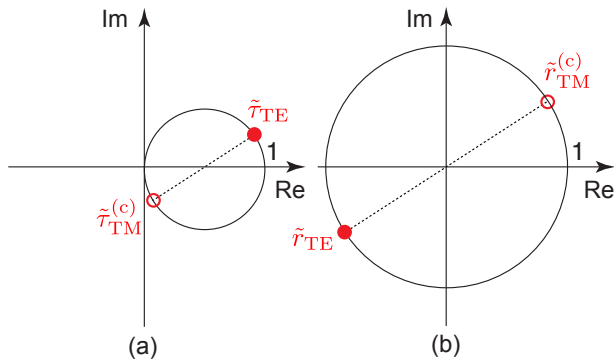


FIG. 2. (a) Transmission coefficients of the transmissive metasurface and its complementary one on a complex plane. (b) Reflection coefficients of the reflective metasurface and its complementary one on a complex plane.

lossless metals with a transmission coefficient of $\tilde{\tau}$ and reflection coefficient $\tilde{\rho}$, continuity of electric fields on the metasurface requires that $1 + \tilde{\rho} = \tilde{\tau}$ and energy conservation requires that $|\tilde{\tau}|^2 + |\tilde{\rho}|^2 = 1$. These two conditions yield

$$|\tilde{\tau}|^2 + |1 - \tilde{\tau}|^2 = 1, \quad (7)$$

which implies that the transmission coefficient $\tilde{\tau}$ is located on a circle with a radius of $1/2$ and center of $1/2$ on a complex plane. Hence, the transmission coefficients $\tilde{\tau}_{TE}$ and $\tilde{\tau}_{TM}^{(c)}$ for the transmissive metasurfaces as shown in Figs. 1(a) and (b), which require the conventional Babinet's relations given by Eqs. (1) and (2), are located on the opposite sides of the circle, as shown in Fig. 2(a). As clearly shown in Fig. 2(a), the transmissive metasurfaces suffer from reduced transmission for large transmission phases $\arg(\tilde{\tau})$. This substantially restricts the efficiency of the wave plate operation, which requires large phase retardation between two polarizations. The reduction in transmission is attributed to the reflection loss. By contrast, the reflection coefficient \tilde{r} of an arbitrary reflective metasurface composed of planar lossless metals and reflection mirror satisfies $|\tilde{r}| = 1$ because all incident energy is reflected by the metasurfaces following the interaction between the metallic structures and the mirror. From Eq. (4), the transmission coefficients $\tilde{\tau}_{TE}$ and $\tilde{\tau}_{TM}^{(c)}$ of the transmissive metasurfaces are mapped onto the corresponding reflection coefficients \tilde{r}_{TE} and $\tilde{r}_{TM}^{(c)}$, as shown in Fig. 2(b). It is confirmed that Babinet's relation extended to the reflective metasurfaces, which is given by Eq. (5), is satisfied. In contrast to transmissive metasurfaces, the reflectances of the reflective metasurfaces are always unity regardless of the phase of reflection, and polarization manipulation with a high efficiency can be expected.

III. HALF-WAVE PLATE USING REFLECTIVE METASURFACE EMBEDDING SELF-COMPLEMENTARY STRUCTURES

A. Babinet's relations for reflective metasurface embedding self-complementary structures

If a structure is congruent with its complementary structure, it is referred to as a self-complementary structure. A typical example of the self-complementary structure, employed in our experiment, is shown in Fig. 3(a). If the self-complementary structures are embedded in a reflective metasurface as shown in Fig. 3(b), the extended Babinet's relations given by Eqs. (5) and (6) are reduced to

$$\tilde{r}_{TE} + \tilde{r}_{TM} = 0, \quad (8)$$

owing to the self-complementarity $\tilde{r}_{TE} = \tilde{r}_{TE}^{(c)}$ and $\tilde{r}_{TM} = \tilde{r}_{TM}^{(c)}$. This relationship indicates that reflective metasurfaces with self-complementary structures function as half-wave plates, which exhibit a π -phase difference between two orthogonal linear polarizations in a reflection mode. If the diffraction and dissipation losses are negligible, the reflectance is expected to be high, $|\tilde{r}_{TE}| = |\tilde{r}_{TM}| \sim 1$, which leads to the implementation of efficient half-wave plates.

B. Simulations

To confirm the extended Babinet's relation given by Eq. (8), numerical simulations were first conducted using an electromagnetic simulator (CST MW Studio) for the metasurface, as shown in Fig. 3(b). The periodicity is assumed to be $a_1 = a_2 = 200 \mu\text{m}$, and the other dimensions are set to $w_x = 30 \mu\text{m}$, $w_y = 50 \mu\text{m}$, and $d = 100 \mu\text{m}$. We assume that the incident plane and incident angle are the x - z plane and $\theta_i = 45^\circ$, respectively. Under this condition, the lowest diffraction frequency is

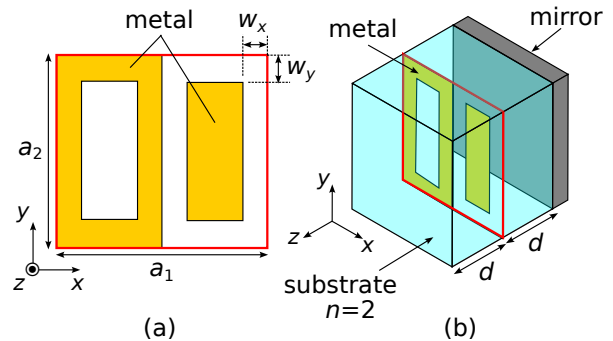


FIG. 3. (a) Unit cell of self-complementary structures composed of planar metallic sheet. (b) Unit cell of reflective metasurface embedding self-complementary structures.

$c_0/a/(1 + \sin \theta_i) = 0.88$ THz. The incident waves are refracted at the angle of $\theta = \sin^{-1}(\sin \theta_i/n) = 20.7^\circ$ in the substrate with the refractive index $n = 2$, and the operating frequency estimated to be $f_0 = 0.40$ THz is derived from $2d = \pi/(k \cos \theta)$. The metal constituting the self-complementary structures was assumed to be aluminum with a thickness of 300 nm, conductivity of 3.56×10^7 S/m, and the mirror was assumed to be gold with a thickness of 200 nm and conductivity of 4.56×10^7 S/m. Floquet boundary conditions were applied along the x - and y -directions to simulate the interaction between the metasurface and the plane waves

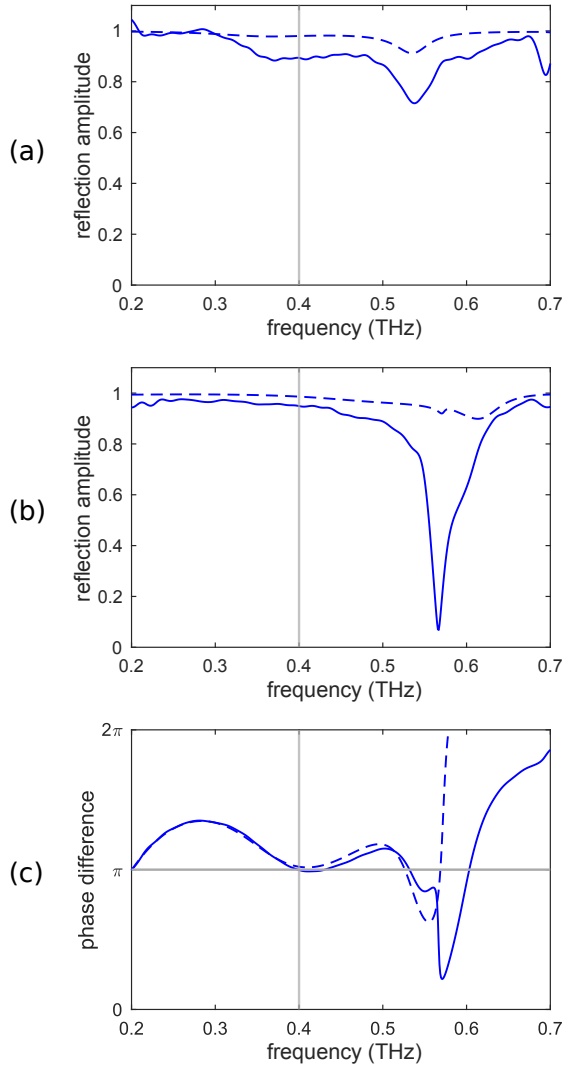


FIG. 4. Amplitude and phase responses of reflective metasurface with $w_x = 30 \mu\text{m}$ and $w_y = 50 \mu\text{m}$. Solid lines and dashed lines represent experimental and simulation results, respectively. (a) Reflection amplitude spectra $|\tilde{r}_{\text{TE}}|$ for TE waves. (b) Reflection amplitude spectra $|\tilde{r}_{\text{TM}}|$ for TM waves. (c) Phase difference $\arg(\tilde{r}_{\text{TE}}/\tilde{r}_{\text{TM}})$ between reflected TE waves and TM waves.

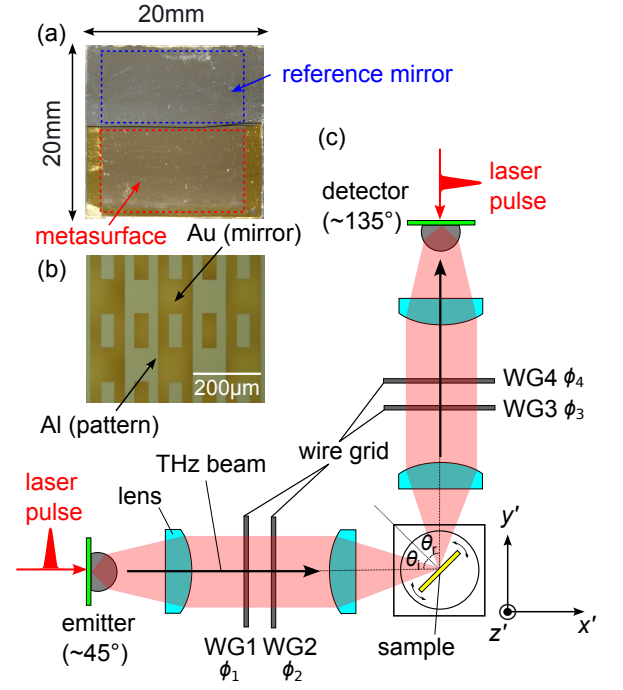


FIG. 5. (a) Photograph of the fabricated sample. (b) Microphotograph of the metasurface parts. (c) Schematics of experimental setup.

incident at $\theta_i = 45^\circ$. The input port was located $1000 \mu\text{m}$ from the top surface of the substrate.

The calculated reflection amplitudes $|\tilde{r}_{\text{TE}}|$ and $|\tilde{r}_{\text{TM}}|$ for the TE and TM waves are indicated by the dashed lines in Figs. 4(a) and (b), respectively. This frequency region, which is lower than the diffraction frequency 0.88 THz, contains no diffraction; consequently, the reflection amplitudes are close to unity. The small depressions observed above 0.50 THz are caused by resonances involving Joule losses in the metallic structures and mirror with finite conductivity. The dashed line in Fig. 4(c) shows the calculated phase difference defined by $\Delta\theta = \arg(\tilde{r}_{\text{TE}}/\tilde{r}_{\text{TM}})$. As expected from the extended Babinet's relationship denoted by Eq. (8), the phase difference between the TE and TM waves approaches π at an operating frequency 0.40 THz, denoted by the gray line. The slight deviation from π is attributed to losses which are not considered in the derivation of Babinet's relation.

C. Experimental demonstration

For the experimental demonstration, synthetic quartz was used as the substrate with a refractive index of $n = 2.0$ [40]. The metasurface was fabricated using the following procedure. First, 10nm-thick titanium and 200nm-thick gold films were deposited as a mirror on a 1mm-thick quartz substrate via electron beam evapora-

tion. Second, the substrate containing the mirror and a thin quartz substrate were bonded with an optical adhesive (Norland, NOA89H). The thickness of the thin quartz substrate was $93\ \mu\text{m}$, and the total thickness including the adhesive layer was $108\ \mu\text{m}$. Third, an aluminum film with a thickness of $300\ \text{nm}$ was deposited via electron beam evaporation. Self-complementary patterns were fabricated via wet etching with a mixture comprised of phosphoric acid, nitric acid, acetic acid, and water, at a 16:1:2:1 ratio, which does not erode the adhesive layer. Next, the patterned substrate was bonded to a thin quartz substrate, whose thickness was $92\ \mu\text{m}$. The distance between the embedded aluminum structures and top surface was $104\ \mu\text{m}$. Finally, a 300-nm -thick aluminum film was deposited on half of the sample to form a reference mirror, which was used to estimate the reflection coefficients. A photograph of the fabricated sample is presented in Fig. 5(a). The reference mirror was placed in the upper half of the sample. The metasurface embedding the self-complementary structures was placed in the lower half of that area. A microphotograph of the metasurface is shown in Fig. 5(b). The white area corresponds to the aluminum patterns that form self-complementary structures, and the gold area corresponds to the mirror made of the gold film, which can be seen through the aluminum structures.

We employed terahertz time-domain spectroscopy (THz-TDS) in the reflective setup as shown in Fig. 5(c) to acquire the reflection spectra of the fabricated metasurface for TE and TM waves. The incident terahertz waves propagate along the x' direction, and the reflected waves from the sample propagate along the y' direction. In this experiment, the incident angle θ_i and reflection angle θ_r were fixed at $\theta_i = \theta_r = 45^\circ$. We introduce polarization angles of ϕ_i and ϕ_r for the incident waves and reflected waves, respectively. The polarization directions are defined as $\cos\phi_i\hat{e}_{y'} + \sin\phi_i\hat{e}_{z'}$ for the incident waves and $\cos\phi_r\hat{e}_{x'} + \sin\phi_r\hat{e}_{z'}$ for the reflected waves, where $\hat{e}_{x'}$, $\hat{e}_{y'}$, and $\hat{e}_{z'}$ are the unit vectors along the x' , y' , and z' directions, respectively. According to this definition, when the incident waves with polarization $\phi_i = 45^\circ$ are reflected by a uniform mirror, the reflected waves have the polarization of $\phi_r = 45^\circ$.

The gaps between electrodes of photoconductive antennas used as the emitter and detector were approximately aligned at 45° and 135° , respectively. The transmission axes of the four wire grids labelled WG1, WG2, WG3, and WG4 are represented as ϕ_1 , ϕ_2 , ϕ_3 , and ϕ_4 , respectively. We fixed $\phi_1 = 45^\circ$ and $\phi_4 = 135^\circ$ and changed the orientations of WG2 and WG3 depending on the polarizations to be measured. We set $\phi_2 = \phi_3 = 90^\circ$ for the TE wave measurement and $\phi_2 = \phi_3 = 0^\circ$ for the TM wave measurement. The collimated terahertz waves were focused using a lens with a focal length of $50\ \text{mm}$, and the beam diameter of the focused waves at the sample position was $1.7\ \text{mm}$, which was much smaller than the areas of the reference mirror and metasurface.

The sample was mounted on a translation stage along

the z' direction. The reflection signals from the reference mirror $r_{\text{ref}}(t)$ and those from the metasurface $r_{\text{meta}}(t)$ were acquired by moving the sample vertically. The reflection coefficients were obtained as $\tilde{r}(\omega) = -\tilde{r}_{\text{meta}}(\omega)/\tilde{r}_{\text{ref}}(\omega)$, where $\tilde{r}_{\text{ref}}(\omega)$ and $\tilde{r}_{\text{meta}}(\omega)$ represent the Fourier transforms of $r_{\text{ref}}(t)$ and $r_{\text{meta}}(t)$, respectively. The negative sign was required because the reference signals $r_{\text{ref}}(t)$ include the effect of electric-field inversion at the mirror. The experimental results of the reflection amplitudes for the TE waves $|\tilde{r}_{\text{TE}}|$ and the TM waves $|\tilde{r}_{\text{TM}}|$ are represented by solid lines in Figs. 4(a) and (b), respectively. The obtained reflection amplitudes at the operating frequency of $0.40\ \text{THz}$ were $|\tilde{r}_{\text{TE}}| = 0.89$ and $|\tilde{r}_{\text{TM}}| = 0.95$. The experimental results exhibited resonance features above $0.5\ \text{THz}$, which led to a significant reduction in the reflection. The dissipation was mainly caused by the dielectric loss of the adhesive layers, which were not considered in the simulations. The solid line in Fig. 4(c) shows the phase difference $\Delta\theta = \arg(\tilde{r}_{\text{TE}}/\tilde{r}_{\text{TM}})$ derived from the experimental results. The experimental (solid line) and simulation results (dashed line) are in good agreement except at the resonant frequencies above $0.5\ \text{THz}$. As expected, the phase difference at the operating frequency $0.40\ \text{THz}$ approached π . The discrepancy around the resonance is mainly attributed to dielectric losses, as discussed above.

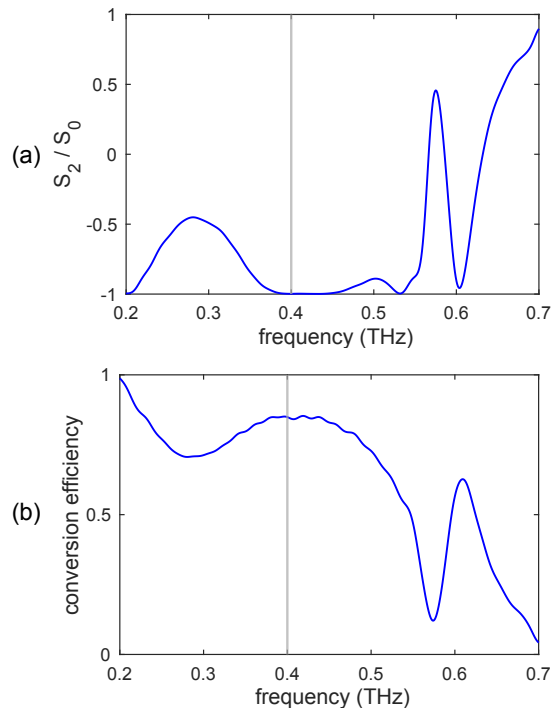


FIG. 6. Polarization property of waves reflected from the reflective metasurface with $w_x = 30\ \mu\text{m}$ and $w_y = 50\ \mu\text{m}$ for incident waves with 45° polarization. (a) Normalized Stokes S_2/S_0 . (b) Polarization conversion efficiency from $\phi_i = 45^\circ$ to $\phi_r = 135^\circ$.

To estimate the performance of the metasurface as a half-wave plate, we analyzed the amplitude and polarization of output waves for incident waves with 45° polarization ($\phi_i = 45^\circ$). Polarization can be characterized by the Stokes parameters [41]; we considered two Stokes parameters, S_0 and S_2 , which can be calculated as

$$S_0 = \frac{|\tilde{r}_{\text{TE}}|^2 + |\tilde{r}_{\text{TM}}|^2}{2}, \quad S_2 = \text{Re}(\tilde{r}_{\text{TE}}^* \tilde{r}_{\text{TM}}), \quad (9)$$

where S_0 denotes the total flux of the output waves and S_2 represents the flux difference between 45° polarization and 135° polarization. The normalized Stokes parameter defined by S_2/S_0 represents the polarization purity, which becomes -1 when the polarization of the output waves is oriented along 135° , that is $\phi_r = 135^\circ$. Figure 6(a) shows the normalized Stokes parameter S_2/S_0 calculated using experimental results. At the operating frequency denoted by the gray line, S_2/S_0 becomes -1 as expected, which validates that the metasurface functions as a half-wave plate with an ideal phase difference.

Next, we consider polarization conversion efficiency η from $\phi_i = 45^\circ$ to $\phi_r = 135^\circ$. Reflection coefficients are introduced as \tilde{r}_{co} for $\phi_r = 45^\circ$ and \tilde{r}_{cr} for $\phi_r = 135^\circ$, and the Stokes parameters of the reflected waves are given as $S_0 = |\tilde{r}_{\text{co}}|^2 + |\tilde{r}_{\text{cr}}|^2$ and $S_2 = |\tilde{r}_{\text{co}}|^2 - |\tilde{r}_{\text{cr}}|^2$ [41]. The polarization conversion efficiency η can be calculated as

$$\eta \equiv |\tilde{r}_{\text{cr}}|^2 = \frac{S_0 - S_2}{2}. \quad (10)$$

Figure 6(b) shows the η derived from the experimental results. The conversion efficiency at the operating frequency, denoted by the gray line, was estimated to be 0.85. It was confirmed that the pure polarization of $\phi_r = 135^\circ$ was achieved with a relatively high conversion efficiency despite the simple implementation of the metasurface using adhesives to bond the substrates. A higher conversion efficiency can be realized using an adhesive-free bonding technique such as room-temperature bonding between metallic films [42].

IV. SIMULTANEOUS CONTROL OF WAVEFRONT AND POLARIZATION

A. Design of phase-gradient metasurface

The extended Babinet's relation expressed in Eq. (8) holds for reflective metasurfaces embedding arbitrary self-complementary structures. The phase difference is always π , however, either phase $\arg(\tilde{r}_{\text{TE}})$ or $\arg(\tilde{r}_{\text{TM}})$ can be freely selected by designing the self-complementary structures. If the self-complementary structures depend on the position x and $\arg(\tilde{r}_{\text{TE}})$ has a constant phase gradient $d\{\arg(\tilde{r}_{\text{TE}})\}/dx \neq 0$, incident TE waves are reflected at anomalous angles that are different from the normal reflection angle on a flat mirror [43]. The phase gradient of the reflected TM waves is identical to that of

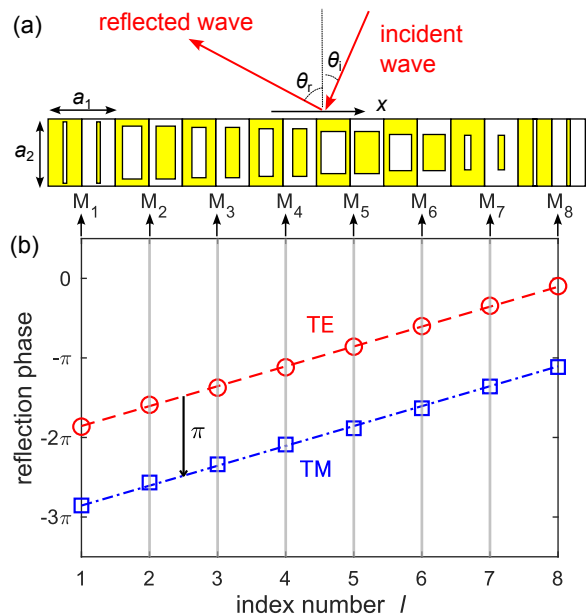


FIG. 7. (a) Unit cell (supercell) of the phase-gradient reflective metasurface composed of eight elements M_l . (b) Reflection phases of each element M_l for TE and TM waves.

the reflected TE waves because of the extended Babinet's relation Eq. (8). Consequently, the TM waves are also reflected at the same anomalous angle. In the process of the anomalous reflection, the function as a half-wave plate, that is, $\arg(\tilde{r}_{\text{TE}}) - \arg(\tilde{r}_{\text{TM}}) = \pi$, is maintained. Hence, the phase-gradient metasurface simultaneously achieves anomalous reflection and polarization control by tailoring the phase response for either the TE or TM waves. Figure 7(a) shows a unit supercell composed of eight elements labeled as $M_l (l = 1, 2, \dots, 8)$, with the same design as that shown in Fig. 3(a) for various design parameters w_x and w_y . If the reflection phase ψ_l for M_l is adjusted to satisfy $\psi_l = \pi l/4 + \psi'$ (ψ' : constant), which provides a phase difference of 2π at both ends of the supercell, the anomalous reflection angle θ_r for the incident angle θ_i is determined using the following generalized Snell's law:

$$p(\sin \theta_i - \sin \theta_r) = -\lambda_0, \quad (11)$$

where p is the periodicity of the supercell and λ_0 is the wavelength in vacuum [18]. For a general periodic structure with periodicity p , the diffraction angles θ_r of m -th order are determined by

$$p(\sin \theta_i - \sin \theta_r) = m\lambda_0. \quad (12)$$

For a phase-gradient metasurface satisfying Eq. (11), the reflection with a diffraction order $m = -1$ is expected. For experimental demonstration using the THz-TDS setup shown in Fig. 5(c), which requires $\theta_i + \theta_r = 90^\circ$, the parameters were set as follows: $a_1 = a_2 = 200 \mu\text{m}$, $p = 8a_1 = 1600 \mu\text{m}$, and $d = 100 \mu\text{m}$, which lead to $\theta_i = 24.8^\circ$ and $\theta_r = 65.2^\circ$ for an operating frequency of $f_0 = 0.384 \text{ THz}$.

TABLE I. Design parameters w_x and w_y for each element M_l comprising the phase-gradient reflective metasurface.

	M_1	M_2	M_3	M_4	M_5	M_6	M_7	M_8
w_x (μm)	44	20	28	28	12	16	40	44
w_y (μm)	8	20	24	28	36	44	48	0

Numerical simulations of the metasurfaces were conducted using the same setup as in Fig. 3(b) for the incident angle $\theta_i = 24.8^\circ$, changing w_x from 0 to 48 μm and w_y from 0 to 96 μm in increments of 4 μm and singled out eight sets of w_x and w_y from the 325 parameter sets to satisfy the linear phase gradient expressed as $\psi_l = \pi l/4 + \psi'$. The parameter sets are listed in Table I, and the calculated reflection phases for the elements M_l are denoted by circles and squares for the TE and TM waves, respectively, in Fig. 7(b). The dashed line was obtained by fitting the reflection phases ψ_l for the TE waves with $\psi_l = \pi l/4 + \psi'$. The dashed-dotted line was obtained by shifting the dashed line by $-\pi$. The reflection phases denoted by the squares are well aligned with the dashed-dotted line, which implies that each element works as a half-wave plate owing to the self-complementary structures satisfying Eq. (8). Because the phase gradients of the reflected TE and TM waves are identical, waves incident at $\theta_i = 24.8^\circ$ with arbitrary polarization are reflected anomalously at $\theta_r = 65.2^\circ$ while acquiring a π -phase difference between the TE and TM wave components.

B. Simulations of anomalous reflection and polarization conversion

Subsequently, we performed numerical simulations for the entire metasurface with the supercell as shown in Fig. 7(a), and obtained all the reflection coefficients for every diffraction mode. Figures 8(a) and (b) represent the reflectances to possible diffraction modes, which are limited from $m = -1$ to $m = 3$ below 0.5 THz, for TE and TM waves, respectively. The reflectances for $m = -1$ correspond to the designed anomalous reflection, and reflection angle is $\theta_r = 65.2^\circ$ at the operating frequency $f_0 = 0.384$ THz denoted by gray lines. For both polarizations, the reflectances for $m = -1$ were maximized at approximately 0.4 THz, while the reflections of the other modes were significantly suppressed. The difference between the designed frequency $f_0 = 0.384$ THz and the optimal frequency ~ 0.4 THz can be attributed to interactions between neighboring elements that were not considered in the design procedure for obtaining the linear phase gradient in the simulation. The reflections of the other modes can be further suppressed by increasing the number of elements in the supercell to obtain a smoother phase gradient.

We can estimate the polarization of the anomalously reflected waves for the incident waves with 45° polar-

ization using Stokes parameters defined in Eq. (9) with the reflection coefficients for the $m = -1$ mode. Figure 9(a) shows a normalized Stokes parameter S_2/S_0 for the $m = -1$ mode. The value of S_2/S_0 is -0.97 at the operating frequency of $f_0 = 0.384$ THz denoted by the gray line, which implies that the difference between the reflection phases for the TE and TM modes was close to π . Figure 9(b) shows a conversion efficiency η_s from incident waves with 45° polarization to anomalously reflected waves ($m = -1$) with 135° polarization. The conversion efficiency η_s was estimated to be 0.85 at the operating frequency of $f_0 = 0.384$ THz denoted by the gray line. These simulation results validate that the wavefront control could be achieved while maintaining its function as a half-wave plate.

C. Experimental demonstration of anomalous reflection and polarization conversion

We fabricated a reflective metasurface using the parameters listed in Table I using the procedure described in Sec. III. A microphotograph of the fabricated metasurface is presented in Fig. 10(a). We conducted an experiment using the THz-TDS system shown in Fig. 5(c) to evaluate the polarization conversion efficiency η_e from waves incident at $\theta_i = 24.8^\circ$ with a polarization of $\phi_i = 45^\circ$ to waves anomalously reflected at $\theta_r = 65.2^\circ$ with a polarization of $\phi_r = 135^\circ$. The angles of wire grids

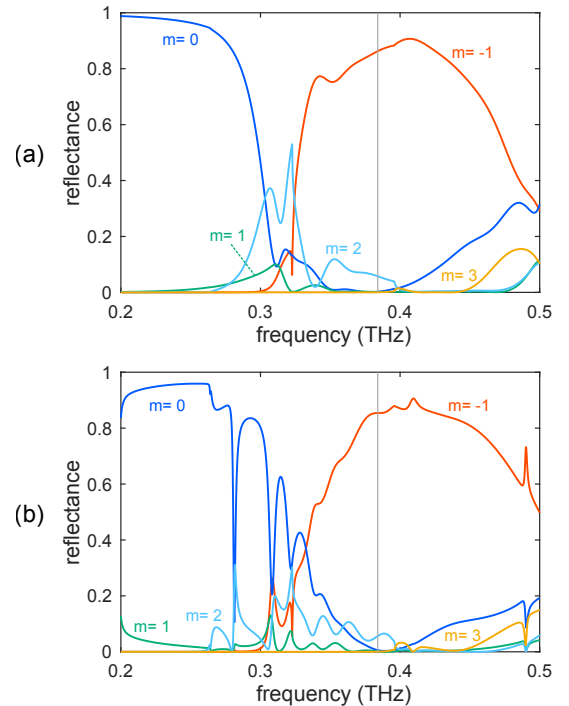


FIG. 8. Reflectances to diffraction modes $m = -1, 0, 1, 2, 3$ for (a) TE waves and (b) TM waves.

WG1, WG2, WG4 were fixed at $\phi_1 = 45^\circ$, $\phi_2 = 45^\circ$, and $\phi_4 = 90^\circ$, respectively. Under this condition, the polarization of the incident waves was fixed at $\phi_i = 45^\circ$.

Prior to measuring the anomalous reflection on the metasurface, we estimated the reference signal $r_{\text{ref}}(t)$ using a flat mirror on the upper half of the sample under the condition where the incident angle θ_i , reflection angle θ_r , and angle of WG3 ϕ_3 , were 45° . The flat mirror reflected the incident waves while maintaining a polarization of $\phi_r = 45^\circ$, which passes through WG3 at $\phi_3 = 45^\circ$. The polarization of the waves from WG3 was projected along $\phi_4 = 90^\circ$ by WG4, and projected at 135° by the detector. As a result, the amplitude decreased by a factor of two after WG3. The obtained signal is denoted as $r_{\text{ref}}(t)$.

Next, the angle of WG3 was changed to $\phi_3 = 135^\circ$. We rotated the sample holder to satisfy $\theta_i = 24.8^\circ$ and $\theta_r = 65.2^\circ$. The sample holder was moved vertically until the incident waves interacted with the metasurface. Incident waves with a polarization of $\phi_i = 45^\circ$ interacted with the metasurface at an angle of $\theta_i = 24.8^\circ$ and were anomalously reflected at an angle of $\theta_r = 65.2^\circ$. A component with a polarization of 135° was selected from the anomalously reflected waves when the waves passing through WG3 aligned along $\phi_3 = 135^\circ$. The polarization of the waves from WG3 was projected along

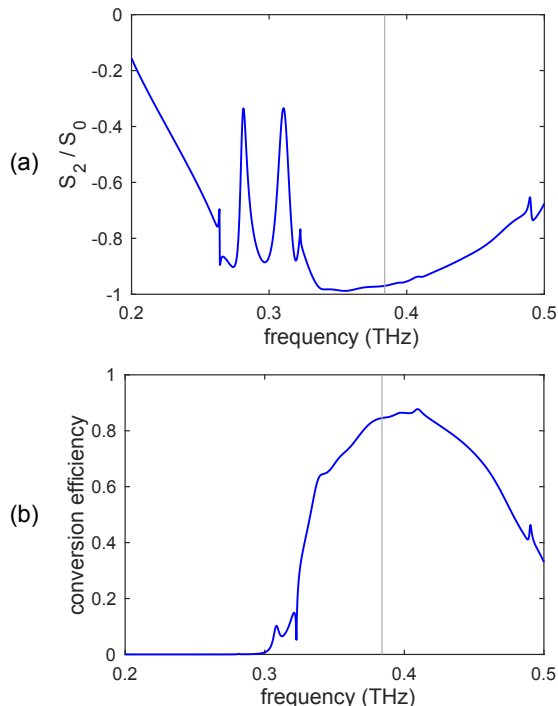


FIG. 9. Polarization property of reflected waves in the $m = -1$ mode for incident waves with an illumination angle of $\theta_i = 24.8^\circ$ and polarization of $\phi_i = 45^\circ$. (a) Normalized Stokes parameter S_2/S_0 . (b) Polarization conversion efficiency η_s from $\phi_i = 45^\circ$ to $\phi_r = 135^\circ$.

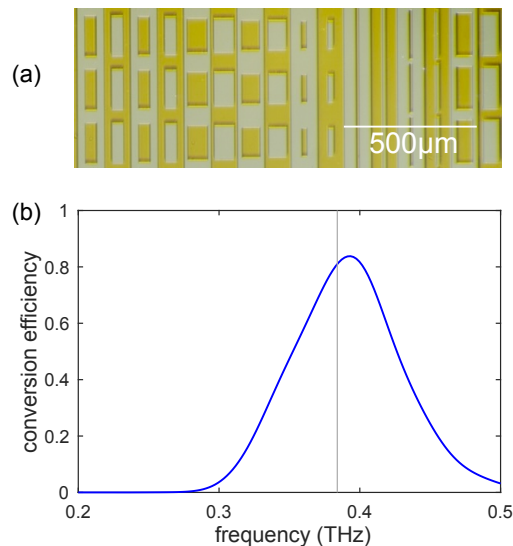


FIG. 10. (a) Microphotograph of the fabricated phase-gradient metasurface. (b) Polarization conversion efficiency η_e from the incident waves with $\theta_i = 24.8^\circ$ and $\phi_i = 45^\circ$ to anomalously reflected waves with $\theta_r = 65.2^\circ$ and $\phi_r = 135^\circ$.

$\phi_4 = 90^\circ$ by WG4, and projected at 135° by the detector. The amplitude decreased by a factor of two after WG3. The signal obtained is defined as $r_{\text{meta}}(t)$. From $\tilde{r}_{\text{meta}}(\omega)$ and $\tilde{r}_{\text{ref}}(\omega)$, which are Fourier transforms of $r_{\text{meta}}(t)$ and $r_{\text{ref}}(t)$, respectively, the conversion efficiency can be estimated as $\eta_e = |\tilde{r}_{\text{meta}}(\omega)/\tilde{r}_{\text{ref}}(\omega)|^2$, which includes the polarization conversion efficiency from $\phi_i = 45^\circ$ to $\phi_r = 135^\circ$ and diffraction efficiency from $\theta_i = 24.8^\circ$ to $\theta_r = 65.2^\circ$.

The conversion efficiency η_e obtained from the experimental results is shown in Fig. 10(b). The value of η_e at the operating frequency of $f_0 = 0.384$ THz was estimated to be 0.81. The optimal frequency was blue-shifted from $f_0 = 0.384$ THz. This deviation can be attributed to interactions between neighboring elements. Note that the definitions of conversion efficiencies η_s and η_e differ. While η_s in the simulation is defined for a specific diffraction order $m = -1$ given by Eq. (12), thus providing a frequency-dependent diffraction angle, η_e in the experiment is defined for a fixed reflection angle of $\theta_r = 65.2^\circ$. The definitions of η_s and η_e coincide only at the operating frequency of $f_0 = 0.384$ THz. Therefore, the shape shown in Fig. 9(b) differs from that of Fig. 10(b).

Compared with previous studies on phase-gradient reflective metasurfaces with similar functions that realize a π -phase difference between two linear polarizations by adjusting the shapes of unit structures [21, 22], the proposed metasurface always functions as a half-wave plate according to the extended Babinet's relations. Hence, only one of the TE- or TM-wave reflection phases need to be controlled by adjusting the dimension of the self-complementary structures.

Previous research based on conventional Babinet's

relations demonstrated a phase-gradient transmissive metasurface with self-complementary structures, which separates incident beams into two non-diffracted beams and two anomalously diffracted beams depending on the circular polarizations [44]. In contrast, the phase-gradient refractive metasurface proposed in this paper reflects most incident waves in an anomalous direction with an accompanying π -phase difference between the two linear polarizations.

V. CONCLUSION

We extended the conventional Babinet's relations derived for transmissive metasurfaces to those of reflective metasurfaces embedding planar metallic structures in a substrate with a reflection mirror. We proposed two types of reflective metasurfaces embedding self-complementary structures as applications of the extended Babinet's relations, which guarantee π -phase difference between the two orthogonal linear polarizations. We have theoretically and experimentally demonstrated a metasurface-based half-wave plate with a reflective metasurface that included single self-complementary structures in the terahertz region. We also designed a reflective metasurface embedding self-complementary structures with a phase gradient in the reflection, and demonstrated simultaneous implementation of anomalous reflection and polarization conversion with high efficiency. The absorption loss caused mainly by the adhesive layers could be reduced by using an adhesive-free bonding technique such as the room-temperature bonding between metallic films [42]. The Joule loss in the metallic structures might be a problem especially in higher frequency regions including optical regime. In fact, deviations from Babinet's relations have been discussed for transmissive metasurfaces [45, 46]. The similar discussion might be applied to the reflective metasurfaces, because Eq. (4) remains valid even in the presence of the Joule loss. The reflections of the undesired diffraction modes can be further suppressed by increasing the number of elements in the supercell to obtain a smoother phase gradient or optimizing the entire structure by considering the interactions among the constituting elements.

In our design of the reflective metasurfaces, the metallic structures are assumed to be embedded in the substrate, because the conventional Babinet's relations are rigorously justified for the structures in a uniform medium. Actually, Babinet's relations for transmissive metasurfaces are empirically valid even for metallic structures placed on the top of a substrate. It might be possible to approximately realize the extended Babinet's relations without embedding metallic structures in substrates, but such implementation is beyond the scope of this paper.

In this paper, we focused on static reflective metasurfaces with self-complementary structures to verify the extended Babinet's relation given by Eq. (8), which is

a special case satisfying $\tilde{r}_{\text{TE}} = \tilde{r}_{\text{TE}}^{(c)}$ and $\tilde{r}_{\text{TM}} = \tilde{r}_{\text{TM}}^{(c)}$ in Eqs. (5) and (6). If the planar structures embedded in the substrate can be converted to their complementary ones, the general Babinet's relations given by Eqs. (5) and (6) can be demonstrated. In fact, reconfigurable polarization devices with transmissive metasurfaces, whose structures can be switched between the original and complementary structures, have been demonstrated by employing conventional Babinet's relations given by Eqs. (1) and (2) [29, 30]. These approaches can be applied to the reflective metasurfaces proposed in this study. The extended Babinet's relations may pave the way for applications in highly efficient multifunctional metasurfaces such as reconfigurable intelligent surfaces [34–37] and polarization-encoded metasurfaces [38, 39]. In addition, the relationship expressed by Eq. (4), which is valid for any planar metallic structures under the derived conditions, could be utilized for novel design of reflective metasurfaces by incorporating the design strategy for transmissive metasurfaces.

ACKNOWLEDGMENTS

We thank Y. Nakata, Y. Urade, K. Takano, and F. Miyamaru for helpful discussions and suggestions. The fabrication of the samples was conducted with the help of Kyoto University Nanotechnology Hub in "Advanced Research Infrastructure for Materials and Nanotechnology Project" sponsored by the Ministry of Education, Culture, Sports, Science and Technology (MEXT), Japan. This work was supported by JSPS KAKENHI (Grants No. 23K04612).

Appendix A: Reflection coefficient of reflective metasurface for normal incidence

To express \tilde{r}_i as a function of $\tilde{\tau}_i$ and $\tilde{\rho}_i$, we calculated the transfer matrix T_i , defined as

$$\begin{pmatrix} E_2^+ \\ E_2^- \end{pmatrix} = T_i \begin{pmatrix} E_1^+ \\ E_1^- \end{pmatrix} = \begin{pmatrix} T_{11} & T_{12} \\ T_{21} & T_{22} \end{pmatrix} \begin{pmatrix} E_1^+ \\ E_1^- \end{pmatrix}, \quad (\text{A1})$$

which connects electric fields E_1^+ and E_1^- at the substrate surface with electric fields E_2^+ and E_2^- immediately be-

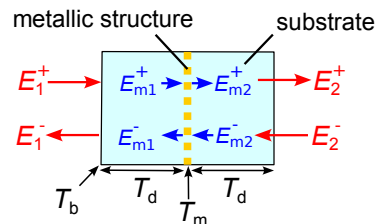


FIG. 11. Transfer-matrix elements from the top surface of the substrate to the bottom end of the substrate.

fore the mirror, as defined in Fig. 11. The transfer matrix can be decomposed into three elements: transfer matrix T_b at the boundary between the vacuum and substrate; T_d characterizing the propagation in the substrate of the length d ; T_m on the metallic structures. T_b and T_d are given as

$$T_b = \frac{1}{2n} \begin{pmatrix} n+1 & n-1 \\ n-1 & n+1 \end{pmatrix}, \quad (\text{A2})$$

$$T_d = \begin{pmatrix} e^{-jkd} & 0 \\ 0 & e^{jkd} \end{pmatrix}, \quad (\text{A3})$$

where n is the substrate refractive index and k is the wavenumber in the substrate. The scattered electric fields from the metallic structures satisfy $E_{m2}^+ = \tilde{\tau}_i E_{m1}^+ + \tilde{\rho}_i E_{m2}^-$ and $E_{m1}^- = \tilde{\rho}_i E_{m1}^+ + \tilde{\tau}_i E_{m2}^-$, where E_{m1}^+ and E_{m1}^- (E_{m2}^- and E_{m2}^+) represent incoming and outgoing waves on the left (right) side of the structures respectively, as shown in Fig. 11, and the transfer matrix T_m is given as follows [41]:

$$T_m = \frac{1}{\tilde{\tau}_i} \begin{pmatrix} \tilde{\tau}_i^2 - \tilde{\rho}_i^2 & \tilde{\rho}_i \\ -\tilde{\rho}_i & 1 \end{pmatrix}. \quad (\text{A4})$$

If d is assumed to be one-fourth the wavelength in the medium, that is $kd = \pi/2$, then the whole transfer matrix given by $T_i = T_d T_m T_b$ is expressed as

$$T_i = \frac{1}{2n\tilde{\tau}_i} \begin{pmatrix} -(n+3)\tilde{\tau}_i + 2 & -(n-3)\tilde{\tau}_i - 2 \\ -(n+1)\tilde{\tau}_i + 2 & -(n-1)\tilde{\tau}_i - 2 \end{pmatrix}. \quad (\text{A5})$$

In this calculation, we used $1 + \tilde{\rho}_i = \tilde{\tau}_i$, which is derived from the electric field continuity at the metallic structures. The boundary condition at the mirror surface requires that $E_2^+ + E_2^- = 0$. The reflection coefficient of the metasurface can be derived as

$$\tilde{r}_i = -\frac{T_{11} + T_{21}}{T_{12} + T_{22}} = -\frac{(n+2)\tilde{\tau}_i - 2}{(n-2)\tilde{\tau}_i + 2}. \quad (\text{A6})$$

Appendix B: Proof for the case of oblique incidence

Under the condition of no scattering to diffraction modes, the electromagnetic property of metasurfaces is effectively described by surface impedance or surface admittance [13]. For the metasurface with uniform structures, the transmission coefficient for normal incidence is written as

$$\tilde{\tau} = \frac{2\bar{Z}}{2\bar{Z} + Z}, \quad (\text{B1})$$

where Z denotes the wave impedance of the surrounding medium and \bar{Z} is the surface impedance of the metasurface. If the structures are anisotropic along the x and y directions, as shown in Figs. 1(a) or (b), the surface impedances in the x and y directions can be defined as \bar{Z}_{TM} and \bar{Z}_{TE} , respectively. Additionally, if the incident

waves are illuminated at an oblique angle θ , the effective wave impedances should be modified to $Z/\cos\theta$ and $Z\cos\theta$ for TE and TM waves, respectively. As a result, the transmission coefficients for the TE and TM waves are respectively expressed as

$$\tilde{\tau}_{TE} = \frac{2\bar{Z}_{TE}\cos\theta}{2\bar{Z}_{TE}\cos\theta + Z}, \quad \tilde{\tau}_{TM} = \frac{2\bar{Z}_{TM}}{2\bar{Z}_{TM} + Z\cos\theta}. \quad (\text{B2})$$

Similarly, the surface impedances of the complementary structures are introduced as $\bar{Z}_{TE}^{(c)}$ and $\bar{Z}_{TM}^{(c)}$ for TE and TM waves, respectively, and the transmission coefficients can be expressed as

$$\tilde{\tau}_{TE}^{(c)} = \frac{2\bar{Z}_{TE}^{(c)}\cos\theta}{2\bar{Z}_{TE}^{(c)}\cos\theta + Z}, \quad \tilde{\tau}_{TM}^{(c)} = \frac{2\bar{Z}_{TM}^{(c)}}{2\bar{Z}_{TM}^{(c)} + Z\cos\theta}. \quad (\text{B3})$$

By substituting these expressions into Babinet's relations given by Eqs. (1) and (2), we obtained the following relationship:

$$\bar{Z}_{TE}\bar{Z}_{TM}^{(c)} = \frac{Z^2}{4}, \quad \bar{Z}_{TM}\bar{Z}_{TE}^{(c)} = \frac{Z^2}{4}. \quad (\text{B4})$$

Next, we derived the reflection coefficients \tilde{r}_i ($i = \text{TE, TM}$) for the reflective metasurface shown in Figs. 1(c) and (d) for oblique incidence at the angle of θ_i . Assuming that the refractive angle is θ in the substrate, Snell's law requires that $\sin\theta_i = n\sin\theta$. The transfer matrices T_b at the substrate surface are expressed as

$$T_b = \frac{1}{2n\cos\theta} \begin{pmatrix} \cos\theta_i + n\cos\theta & -\cos\theta_i + n\cos\theta \\ -\cos\theta_i + n\cos\theta & \cos\theta_i + n\cos\theta \end{pmatrix}, \quad (\text{B5})$$

for TE waves and

$$T_b = \frac{1}{2n\cos\theta} \begin{pmatrix} \cos\theta + n\cos\theta_i & -\cos\theta + n\cos\theta_i \\ -\cos\theta + n\cos\theta_i & \cos\theta + n\cos\theta_i \end{pmatrix}, \quad (\text{B6})$$

for TM waves [41]. The transfer matrix for propagation in the substrate is given by

$$T_d = \begin{pmatrix} e^{-jkd\cos\theta} & 0 \\ 0 & e^{jkd\cos\theta} \end{pmatrix}, \quad (\text{B7})$$

for both TE and TM waves. The transfer matrices for the metallic structure T_m can be calculated substituting Eqs. (B2) and (B3) into Eq. (A4) with $1 + \tilde{\rho}_i = \tilde{\tau}_i$. Subsequently, the whole transfer matrices $T_i = T_d T_m T_b$ can be calculated. Similarly, when Eq. (A6) is derived, the reflection coefficients under a condition of $kd\cos\theta = \pi/2$ can be obtained as

$$\tilde{r}_{TE} = \frac{-n^2\bar{Z}_{TE}\cos^2\theta + Z_0\cos\theta_i}{n^2\bar{Z}_{TE}\cos^2\theta + Z_0\cos\theta_i}, \quad (\text{B8})$$

$$\tilde{r}_{TM} = \frac{-n^2\bar{Z}_{TM}\cos\theta_i + Z_0\cos^2\theta}{n^2\bar{Z}_{TM}\cos\theta_i + Z_0\cos^2\theta}, \quad (\text{B9})$$

for TE and TM waves, respectively. The reflection coefficients of the refractive metasurface embedding the complementary structures with the surface impedance $\bar{Z}_{\text{TE}}^{(c)}$ and $\bar{Z}_{\text{TM}}^{(c)}$ are

$$\tilde{r}_{\text{TE}}^{(c)} = \frac{-n^2 \bar{Z}_{\text{TE}}^{(c)} \cos^2 \theta + Z_0 \cos \theta_i}{n^2 \bar{Z}_{\text{TE}}^{(c)} \cos^2 \theta + Z_0 \cos \theta_i}, \quad (\text{B10})$$

$$\tilde{r}_{\text{TM}}^{(c)} = \frac{-n^2 \bar{Z}_{\text{TM}}^{(c)} \cos \theta_i + Z_0 \cos^2 \theta}{n^2 \bar{Z}_{\text{TM}}^{(c)} \cos \theta_i + Z_0 \cos^2 \theta}. \quad (\text{B11})$$

From Eqs. (B8) and (B11), the sum of \tilde{r}_{TE} and $\tilde{r}_{\text{TM}}^{(c)}$ yields

$$\tilde{r}_{\text{TE}} + \tilde{r}_{\text{TM}}^{(c)} = \frac{2 \cos^2 \theta \cos \theta_i (Z_0^2 - n^4 \bar{Z}_{\text{TE}} \bar{Z}_{\text{TM}}^{(c)})}{(n^2 \bar{Z}_{\text{TE}} \cos^2 \theta + Z_0 \cos \theta_i)(n^2 \bar{Z}_{\text{TM}}^{(c)} \cos \theta_i + Z_0 \cos^2 \theta)}. \quad (\text{B12})$$

Using Eq. (B4), which is derived from Babinet's relations and $Z = Z_0/n$, where Z_0 is the wave impedance of vacuum, we obtain

$$Z_0^2 - n^4 \bar{Z}_{\text{TE}} \bar{Z}_{\text{TM}}^{(c)} = Z_0^2 \left(1 - \frac{n^2}{4}\right), \quad (\text{B13})$$

and this factor becomes zero for $n = 2$, which yields $\tilde{r}_{\text{TE}} + \tilde{r}_{\text{TM}}^{(c)} = 0$. Similarly, $\tilde{r}_{\text{TM}} + \tilde{r}_{\text{TE}}^{(c)} = 0$ can be verified under this condition. In summary, the extended Babinet's relations expressed in Eqs. (5) and (6) are satisfied for $n = 2$ and $2d = \pi/k \cos \theta$.

-
- [1] N. Yu and F. Capasso, Flat optics with designer metasurfaces, *Nat. Mater.* **13**, 139 (2014).
- [2] A. E. Minovich, A. E. Miroschnichenko, A. Y. Bykov, T. V. Murzina, D. N. Neshev, and Y. S. Kivshar, Functional and nonlinear optical metasurfaces, *Laser Photonics Rev.* **9**, 195 (2015).
- [3] S. Walia, C. M. Shah, P. Gutruf, H. Nili, D. R. Chowdhury, W. Withayachumnankul, M. Bhaskaran, and S. Sriram, Flexible metasurfaces and metamaterials: A review of materials and fabrication processes at micro- and nano-scales, *Appl. Phys. Rev.* **2**, 011303 (2015).
- [4] W. J. Padilla, Group theoretical description of artificial electromagnetic metamaterials, *Opt. Express* **15**, 1639 (2007).
- [5] M. Kuwata-Gonokami, N. Saito, Y. Ino, M. Kauranen, K. Jefimovs, T. Vallius, J. Turunen, and Y. Svirko, Giant optical activity in quasi-two-dimensional planar nanostructures, *Phys. Rev. Lett.* **95**, 227401 (2005).
- [6] A. V. Rogacheva, V. A. Fedotov, A. S. Schwanecke, and N. I. Zheludev, Giant gyrotropy due to electromagnetic-field coupling in a bilayered chiral structure, *Phys. Rev. Lett.* **97**, 177401 (2006).
- [7] B. Wang, J. Zhou, T. Koschny, M. Kafesaki, and C. M. Soukoulis, Chiral metamaterials: simulations and experiments, *J. Opt. A* **11**, 114003 (2009).
- [8] C. Caloz and A. Sihvola, Electromagnetic chirality, part 1: The microscopic perspective, *IEEE Antennas Propag. Mag.* **62**, 58 (2020).
- [9] C. Caloz and A. Sihvola, Electromagnetic chirality, part 2: The macroscopic perspective, *IEEE Antennas Propag. Mag.* **62**, 82 (2020).
- [10] A. Pors, M. G. Nielsen, G. D. Valle, M. Willatzen, O. Albrektsen, and S. I. Bozhevolnyi, Plasmonic metamaterial wave retarders in reflection by orthogonally oriented detuned electrical dipoles, *Opt. Lett.* **36**, 1626 (2011).
- [11] A. Pors, M. G. Nielsen, and S. I. Bozhevolnyi, Broadband plasmonic half-wave plates in reflection, *Opt. Lett.* **38**, 513 (2013).
- [12] S.-C. Jiang, X. Xiong, Y.-S. Hu, Y.-H. Hu, G.-B. Ma, R.-W. Peng, C. Sun, and M. Wang, Controlling the polarization state of light with a dispersion-free metastructure, *Phys. Rev. X* **4**, 021026 (2014).
- [13] C. Pfeiffer and A. Grbic, Bianisotropic metasurfaces for optimal polarization control: Analysis and synthesis, *Phys. Rev. Applied* **2**, 044011 (2014).
- [14] S. Kruk, B. Hopkins, I. I. Kravchenko, A. Miroschnichenko, D. N. Neshev, and Y. S. Kivshar, Broadband highly efficient dielectric metadevices for polarization control, *APL Photonics* **1**, 030801 (2016).
- [15] Y. Deng, Z. Cai, Y. Ding, S. I. Bozhevolnyi, and F. Ding, Recent progress in metasurface-enabled optical waveplates, *Nanophotonics* **11**, 2219 (2022).
- [16] M. T. Nouman, J. H. Hwang, and J.-H. Jang, Ultrathin terahertz quarter-wave plate based on split ring resonator and wire grating hybrid metasurface, *Sci. Rep.* **6**, 39062 (2016).
- [17] D. Wang, Y. Gu, Y. Gong, C.-W. Qiu, and M. Hong, An ultrathin terahertz quarter-wave plate using planar babinet-inverted metasurface, *Opt. Express* **23**, 11114 (2015).
- [18] N. Yu, P. Genevet, M. A. Kats, F. Aieta, J.-P. Tetienne, F. Capasso, and Z. Gaburro, Light propagation with phase discontinuities: Generalized laws of reflection and refraction, *Science* **334**, 333 (2011).
- [19] F. Ding, A. Pors, and S. I. Bozhevolnyi, Gradient metasurfaces: a review of fundamentals and applications, *Rep. Prog. Phys.* **81**, 026401 (2018).
- [20] D. Lin, P. Fan, E. Hasman, and M. L. Brongersma, Dielectric gradient metasurface optical elements, *Science* **345**, 298 (2014).
- [21] Y. Yang, W. Wang, P. Moitra, I. I. Kravchenko, D. P. Briggs, and J. Valentine, Dielectric meta-reflectarray for broadband linear polarization conversion and optical vortex generation, *Nano Lett.* **14**, 1394 (2014).
- [22] F. Ding, Z. Wang, S. He, V. M. Shalaev, and A. V. Kildishev, Broadband high-efficiency half-wave plate: A

- supercell-based plasmonic metasurface approach, *ACS Nano* **9**, 4111 (2015).
- [23] A. Arbabi, Y. Horie, M. Bagheri, and A. Faraon, Dielectric metasurfaces for complete control of phase and polarization with subwavelength spatial resolution and high transmission, *Nat. Nanotechnol.* **10**, 937 (2015).
- [24] G. Zheng, H. Mühlenbernd, M. Kenney, G. Li, T. Zentgraf, and S. Zhang, Metasurface holograms reaching 80% efficiency, *Nat. Nanotechnol.* **10**, 308 (2015).
- [25] M. Khorasaninejad, W. T. Chen, R. C. Devlin, J. Oh, A. Y. Zhu, and F. Capasso, Metalenses at visible wavelengths: Diffraction-limited focusing and subwavelength resolution imaging, *Science* **352**, 1190 (2016).
- [26] F. Falcone, T. Lopetegi, M. A. G. Laso, J. D. Baena, J. Bonache, M. Beruete, R. Marqués, F. Martín, and M. Sorolla, Babinet principle applied to the design of metasurfaces and metamaterials, *Phys. Rev. Lett.* **93**, 197401 (2004).
- [27] Y. Nakata, Y. Urade, T. Nakanishi, and M. Kitano, Plane-wave scattering by self-complementary metasurfaces in terms of electromagnetic duality and Babinet's principle, *Phys. Rev. B* **88**, 205138 (2013).
- [28] Y. Nakata, Y. Urade, K. Okimura, T. Nakanishi, F. Miyamaru, M. W. Takeda, and M. Kitano, Anisotropic Babinet-invertible metasurfaces to realize transmission-reflection switching for orthogonal polarizations of light, *Phys. Rev. Applied* **6**, 044022 (2016).
- [29] Y. Nakata, K. Fukawa, T. Nakanishi, Y. Urade, K. Okimura, and F. Miyamaru, Reconfigurable terahertz quarter-wave plate for helicity switching based on Babinet inversion of an anisotropic checkerboard metasurface, *Phys. Rev. Applied* **11**, 044008 (2019).
- [30] T. Nakanishi, Y. Nakata, Y. Urade, and K. Okimura, Broadband operation of active terahertz quarter-wave plate achieved with vanadium-dioxide-based metasurface switchable by current injection, *Appl. Phys. Lett.* **117**, 091102 (2020).
- [31] Y. Urade, K. Fukawa, F. Miyamaru, K. Okimura, T. Nakanishi, and Y. Nakata, Dynamic inversion of planar-chiral response of terahertz metasurface based on critical transition of checkerboard structures, *Nanophotonics* **11**, 2057 (2022).
- [32] Y. Urade, Y. Nakata, T. Nakanishi, and M. Kitano, Frequency-independent response of self-complementary checkerboard screens, *Phys. Rev. Lett.* **114**, 237401 (2015).
- [33] J. D. Baena, J. P. del Risco, A. P. Slobozhanyuk, S. B. Glybovski, and P. A. Belov, Self-complementary metasurfaces for linear-to-circular polarization conversion, *Phys. Rev. B* **92**, 245413 (2015).
- [34] F. Yang, P. Pitchappa, and N. Wang, Terahertz reconfigurable intelligent surfaces (RISs) for 6G communication links, *Micromachines* **13**, 285 (2022).
- [35] L. Li, H. Zhao, C. Liu, L. Li, and T. J. Cui, Intelligent metasurfaces: control, communication and computing, *eLight* **2**, 7 (2022).
- [36] P. Lin, C. Qian, J. Zhang, J. Chen, X. Zhu, Z. Wang, J. Huangfu, and H. Chen, Enabling intelligent metasurfaces for semi-known input, *PIER* **178**, 83 (2023).
- [37] L. Jin, J. Xie, B. Pan, and G. Luo, Generalized phase retrieval model based on physics-inspired network for holographic metasurface, *PIER* **178**, 103 (2023).
- [38] G.-Y. Lee, J. Sung, and B. Lee, Recent advances in metasurface hologram technologies, *ETRI J.* **41**, 10 (2019).
- [39] F. Ding, S. Tang, and S. I. Bozhevolnyi, Recent advances in polarization-encoded optical metasurfaces, *Adv. Photonics Res.* **2**, 2000173 (2021).
- [40] M. Naftaly and R. E. Miles, Terahertz time-domain spectroscopy for material characterization, *Proc. IEEE* **95**, 1658 (2007).
- [41] B. E. A. Saleh and M. C. Teich, *Fundamentals of photonics* (Wiley, New York, NY, 2007).
- [42] M. Kobachi, F. Miyamaru, T. Nakanishi, K. Okimura, A. Sanada, and Y. Nakata, Dynamic quarter-wave metasurface for efficient helicity inversion of polarization beyond the single-layer conversion limit, *Adv. Opt. Mater.* **10**, 2101615 (2021).
- [43] S.-q. Liu, Z.-y. Ma, J. Pei, Q.-b. Jiao, L. Yang, W. Zhang, H. Li, Y.-h. Li, Y.-b. Zou, and X. Tan, A review of anomalous refractive and reflective metasurfaces, *Nano. Prec. Eng.* **5**, 025001 (2022).
- [44] S. A. Kuznetsov, V. A. Lenets, M. A. Tumashov, A. D. Sayanskiy, P. A. Lazorskiy, P. A. Belov, J. D. Baena, and S. B. Glybovski, Self-complementary metasurfaces for designing terahertz deflecting circular-polarization beam splitters, *Appl. Phys. Lett.* **118**, 131601 (2021).
- [45] T. Zentgraf, T. P. Meyrath, A. Seidel, S. Kaiser, H. Giessen, C. Rockstuhl, and F. Lederer, Babinet's principle for optical frequency metamaterials and nanoantennas, *Phys. Rev. B* **76**, 033407 (2007).
- [46] J. D. Ortiz, J. D. Baena, R. Marqués, A. N. Ene-muo, J. Gollub, R. Akhmechet, B. Penkov, C. Sarantos, and D. T. Crouse, Babinet's principle and saturation of the resonance frequency of scaled-down complementary metasurfaces, *Appl. Phys. Lett.* **118**, 221901 (2021).